

## Strong stress-enhanced diffusion in amorphous lithium alloy nanowire electrodes

Y. F. Gao and M. Zhou<sup>a)</sup>

*The George W. Woodruff School of Mechanical Engineering, Georgia Institute of Technology, Atlanta, Georgia 30332-0405, USA*

(Received 20 July 2010; accepted 23 November 2010; published online 10 January 2011)

Diffusion-induced stress (DIS) development and stress-enhanced diffusion (SED) in amorphous lithium alloy nanowire battery electrodes are investigated using a finite deformation model, accounting for full two-way coupling between diffusion and stress evolution. Analytical solutions are derived using a perturbation method. The analyses reveal significant contributions to the driving force for diffusion by stress gradient, an effect much stronger than those seen in cathode lattices but so far has been neglected for alloy-based anodes. The contribution of stress to diffusion is small at low lithium concentrations, this lack of SED leads to significantly higher DIS levels in early stages of a charging cycle. As lithium concentration increases, SED becomes more pronounced, leading to lower DIS levels. The long-term DIS level in the material scales with charging rate, nanowire radius, and the mobility of Li ions as modulated by the effect of stress. The solutions obtained provide guidance for lowering stresses during charging. In particular, lower charging rates should be used during the initial stages of charging cycles. © 2011 American Institute of Physics.

[doi:[10.1063/1.3530738](https://doi.org/10.1063/1.3530738)]

### I. INTRODUCTION

Lithium alloys with metallic or semimetallic elements are attractive candidate materials for the next generation negative electrodes of lithium ion batteries due to their large specific and volumetric capacities.<sup>1</sup>  $\text{Li}_x\text{Si}$  ( $x$  Li atoms per Si) electrodes are particularly interesting because they have the highest known theoretical charge capacity of  $4200 \text{ mAhg}^{-1}$  and can avoid phase boundary strains thanks to their amorphous structures when lithiated at room temperature.<sup>2</sup> The key challenge with lithium alloy electrodes, especially  $\text{Li}_x\text{Si}$ , has been their large volume changes during insertion and extraction of lithium. These volume changes can lead to pulverization and debonding.<sup>3</sup> Recent efforts to improve the cyclability of Li-alloy based electrodes are highlighted by the utilization of nanostructured materials, including Si nanowires (NWs),<sup>4</sup> crystalline-amorphous Si core-shell NWs,<sup>5</sup> sealed Si nanotubes<sup>6</sup> and nanostructured carbon/silicon composites.<sup>7</sup> It is widely accepted that nanosized materials provide better accommodation for diffusion-induced stress (DIS) and thus improve a battery's cyclability.

Phenomenological analyses of the development of DIS have been carried out extensively.<sup>8–14</sup> Christensen and Newman<sup>8</sup> considered the effect of pressure-driven diffusion and nonideal interactions between lithium and host material. Cheng and Verbrugge<sup>10–12</sup> took the analogy with thermally-induced stresses and obtained analytical solutions for a range of nanoparticle shapes. Haftbaradaran *et al.*<sup>15</sup> discussed the condition and effect of surface locking under extremely high DIS. In this paper, we study the fully two-way coupling between stress development and diffusion in an amorphous  $\text{Li}_x\text{Si}$  NW using the large deformation framework of Wu<sup>16</sup> previously used to model selective oxidation of alloys<sup>17,18</sup> and defect migrations in ionic solids.<sup>19,20</sup> At issue is the sig-

nificant contribution of stress gradient to the driving force for diffusion which has hitherto been neglected for amorphous alloy electrodes. We consider the short-term response and the long-term behavior to highlight the important effects at work in different stages of charge/discharge cycles. Analytical solutions are obtained using a perturbation method. Analyses reveal that the short-term response is dominated by very high DIS levels due to the absence of a strong two-way coupling between diffusion and mechanical deformation or the lack of stress-enhanced diffusion (SED) at dilute lithium concentrations. This finding shows that fast initial charging and deep discharging are detrimental to the cyclability of  $\text{Li}_x\text{Si}$  electrodes due to high DIS levels at low Li concentrations. More importantly, the analyses also reveal that the long-term behavior, on the other hand, is determined by strong two-way coupling between diffusion and stress development, due to a SED effect much stronger than those in most intercalation electrodes.<sup>13</sup> Under such conditions, the DIS level scales with the NW radius, charging rate, and the effective diffusivity which accounts for the modulating effect of stress on mass transport. This finding suggests that designs that take advantage of the size effect, controlling of charging rate and enhancement of diffusion through alloying are all effective means for enhancing the reliability of  $\text{Li}_x\text{Si}$  anodes.

Although the analyses are carried out for  $\text{Li}_x\text{Si}$  anodes, the principle and solutions are applicable to any alloy-based electrodes undergoing large deformations during charge/discharge.

### II. LINEAR PERTURBATION RELATIVE TO STRESS-FREE STATE

To analyze the large deformation of  $\text{Li}_x\text{Si}$  during Li insertion, we assume that the host atoms (Si) undergo only convection but negligible diffusion when the problem is treated in a Lagrangian frame fixed on the host. This is the

<sup>a)</sup>Electronic mail: min.zhou@me.gatech.edu.

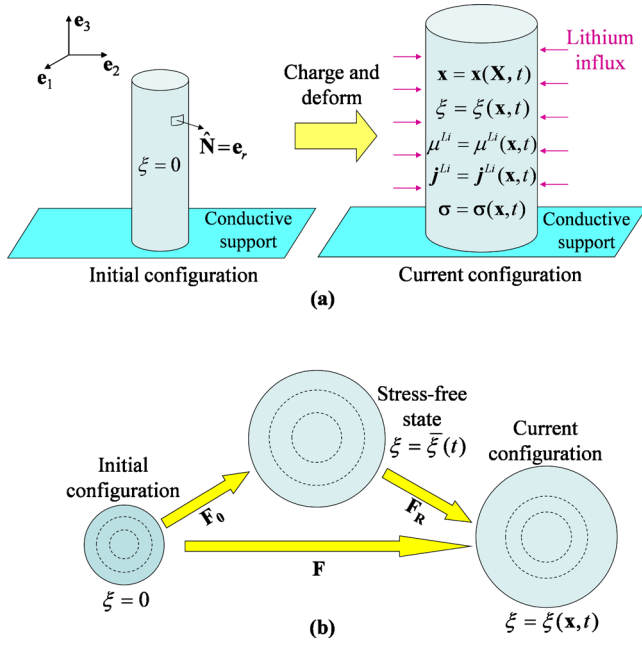


FIG. 1. (Color online) (a) Galvanostatic charging and finite deformation of initially pure Si host NW; (b) Imaginary stress-free configuration.

case for carbon in  $\text{LiC}_6$ , as the carbon atoms form a scaffold through which small Li ions diffuse. It is also a good approximation for  $\text{Li}_\xi\text{Si}$  because the diffusivity of Si is much smaller than that of Li. The motion of the diffusion-inert species of atoms defines the continuum deformation  $\mathbf{x} = \mathbf{x}(\mathbf{X}, t)$ . In an Eulerian frame, the significant difference in diffusivity of Li and Si would lead to an interdiffusion effect similar to the Kirkendall effect. An updated Lagrangian description in which silicon atoms can be treated as immobile, on the other hand, is much simpler and thus preferred. Since the Lagrangian concentration  $C^{\text{Si}}$  of Si is time-independent, it is convenient to use the dimensionless (or normalized) Li concentration  $\xi \equiv C^{\text{Li}}/C^{\text{Si}} = c^{\text{Li}}/c^{\text{Si}}$  to quantify the alloy composition. Here,  $C^{\text{Li}}$  and  $C^{\text{Si}}$  are the Lagrangian concentrations of Li and Si, respectively, while  $c^{\text{Li}}$  and  $c^{\text{Si}}$  are their respective updated Lagrangian counterparts. The flux, on the other hand, can be measured either in the Lagrangian frame as  $\mathbf{J}^{\text{Li}}$  or in the updated Lagrangian frame as  $\mathbf{j}^{\text{Li}}$ . The Lagrangian and updated Lagrangian representations are related by the deformation gradient  $F_{iJ} = \partial x_i / \partial X_J$  through

$$c^{\text{Li}} = \frac{C^{\text{Li}}}{\det(\mathbf{F})} = \frac{C^{\text{Si}}}{\det(\mathbf{F})} \xi \quad \text{and} \quad J_K^{\text{Li}} = \det(\mathbf{F}) \frac{\partial X_K}{\partial x_i} j_i^{\text{Li}}. \quad (1)$$

As illustrated in Fig. 1(a), the electrode analyzed is a free-standing cylindrical NW made of pure Si [ $\text{Li}_\xi\text{Si}$  with  $\xi(r, t)|_{r=0} = 0$ ] with initial radius  $\rho_0$ . The mechanical constraint near the junction between the NW and the conductive support is neglected because the aspect ratio of the NW is assumed to be very large. Under galvanostatic conditions, the Lagrangian surface influx is constant, i.e.,

$$J_s = -\mathbf{e}_r \cdot \mathbf{J}^{\text{Li}} = \frac{1}{2} \rho_0 C^{\text{Si}} \xi_{\text{max}} \frac{1}{T_0}, \quad (2)$$

where  $\xi_{\text{max}} = 4.4$  is the charging limit of  $\text{Li}_\xi\text{Si}$ ,  $T_0$  is the total time required to attain full charge, and  $\mathbf{e}_r$  is the base vector in

the radial direction in a cylindrical coordinate frame and is equal to the unit surface normal  $\hat{\mathbf{N}}$ . The volume average lithium concentration in the NW at time  $t$  is  $\bar{\xi}(t) = \xi_{\text{max}} t / T_0$ .

Lithium flux in the updated Lagrangian frame is determined by Fick's law as

$$j_k^{\text{Li}} = -\frac{D^{\text{Li}}}{k_B \theta} C^{\text{Li}} \frac{\partial \mu^{\text{Li}}}{\partial x_k}, \quad (3)$$

where  $D^{\text{Li}}$  is the diffusion coefficient of lithium in  $\text{Li}_\xi\text{Si}$ ,  $k_B$  is the Boltzmann constant, and  $\theta$  is temperature which is taken to be a constant in this paper ( $\theta = 300$  K). The chemical potential for lithium is<sup>16</sup>

$$\mu^{\text{Li}} = \mu_*^{\text{Li}} + k_B \theta \ln \gamma^{\text{Li}} x^{\text{Li}} - \frac{1}{3} \frac{1}{C^{\text{Si}}} \frac{dJ^{\text{SF}}}{d\xi} \sigma_{kk}, \quad (4)$$

where  $\mu_*^{\text{Li}}$  is the Li chemical potential at the reference state,  $x^{\text{Li}} \equiv \xi / (\xi + 1)$  is the mole fraction of Li and  $\gamma^{\text{Li}}$  is the activity coefficient of Li.  $J^{\text{SF}} = J^{\text{SF}}(\xi)$  is the Jacobian associated with the stress-free volume expansion when the alloy is charged uniformly without mechanical constraint. Here, we use the linear relation  $J^{\text{SF}}(\xi) = 1 + \eta \xi$  which is a good description according to recent findings of Chevrier and Dahn.<sup>2</sup> In particular, since the volume expansion of  $\text{Li}_\xi\text{Si}$  is 311% between  $\xi = 0$  and  $\xi = 4.4$ ,<sup>21</sup>  $\eta = 3.11/4.4 = 0.707$ .

When the wire radius is at the nanometer scale, bulk stress could be affected by surface energy and surface stress.<sup>10,12</sup> In particular, for an infinitely long wire the contribution of the surface stress of  $\boldsymbol{\sigma}^{\text{surf}} = \sigma_\theta^{\text{surf}} \mathbf{e}_\theta \otimes \mathbf{e}_\theta + \sigma_z^{\text{surf}} \mathbf{e}_z \otimes \mathbf{e}_z$  to the bulk stress is:

$$\boldsymbol{\sigma}^0 = -\frac{\sigma_\theta^{\text{surf}}}{\rho} \mathbf{e}_r \otimes \mathbf{e}_r - \frac{\sigma_\theta^{\text{surf}}}{\rho} \mathbf{e}_\theta \otimes \mathbf{e}_\theta - \frac{2\sigma_z^{\text{surf}}}{\rho} \mathbf{e}_z \otimes \mathbf{e}_z, \quad (5)$$

where  $\rho$  is the wire radius in the current configuration. Due to its homogeneous nature,  $\boldsymbol{\sigma}^0$  does not affect the diffusion flux per Eqs. (3) and (4).

We base our analysis on the large deformation theory of Wu,<sup>16</sup> but linearize the equations using a perturbation method in order to obtain analytical solutions for short-time (low concentrations) and long-term (high concentrations) responses. To this end, a homogeneously charged state with  $\xi = \bar{\xi}$ , zero Cauchy stress ( $\boldsymbol{\sigma} = \mathbf{0}$ ) and uniform deformation gradient  $\mathbf{F}_0 = [J^{\text{SF}}(\bar{\xi})]^{1/3} \mathbf{I}$  is taken as an imaginary Lagrangian state from which perturbations are made [cf. Fig. 1(b)]. Here,  $\mathbf{I}$  is the second-order identity tensor. The underlying assumption is that the  $\xi$  field in the NW deviates slightly from the averaged, homogeneous, and stress-free state. If the variation in concentration  $\Delta \xi \equiv \xi - \bar{\xi}$  is small across the NW, the relative deformation gradient  $\mathbf{F}_R \equiv \mathbf{F} \cdot \mathbf{F}_0^{-1}$  between the imaginary configuration represented by  $\mathbf{F}_0$  and the true current configuration whose deformation gradient is  $\mathbf{F}$  should be small. Therefore,  $\mathbf{F}$  is regarded as a perturbation around  $\mathbf{F}_0$  due to  $\Delta \xi$ . All field quantities can be conveniently referred to  $\mathbf{F}_0$  as a first order approximation to their updated Lagrangian representations relative to the true current configuration. The finite deformation constitutive relation<sup>16</sup> can be linearized as

$$\boldsymbol{\varepsilon} = \frac{1+\nu}{E} \boldsymbol{\sigma} - \frac{\nu}{E} \text{tr}(\boldsymbol{\sigma}) \mathbf{I} + \frac{1}{3} \frac{\eta}{J^{SF}(\bar{\xi})} \Delta \xi \mathbf{I}, \quad (6)$$

where  $\boldsymbol{\varepsilon} \equiv (\mathbf{F}_R^T \cdot \mathbf{F}_R - \mathbf{I})/2$  is the Lagrangian strain relative to the uniformly expanded, stress-free configuration,  $E = E(\bar{\xi})$  is the concentration-dependent Young's modulus and  $\nu = \nu(\bar{\xi})$  is the Poisson ratio. In fact, given  $\Delta \xi(r, t) = \xi - \bar{\xi}$ , the stress profiles follow the classical solution in thermoelasticity,<sup>22</sup> i.e.,

$$\left. \begin{aligned} \sigma_z &= -\frac{1}{3} \frac{1}{J^{SF}(\bar{\xi})} \frac{dJ^{SF}}{d\xi} \frac{E}{1-\nu} \cdot \Delta \xi - \frac{2\sigma_z^{surf}}{\rho}, \\ \sigma_\theta &= \frac{1}{3} \frac{1}{J^{SF}(\bar{\xi})} \frac{dJ^{SF}}{d\xi} \frac{E}{1-\nu} \left( -\Delta \xi + \frac{1}{r^2} \int_0^{\tilde{r}} \tilde{r} \Delta \xi d\tilde{r} \right) - \frac{\sigma_\theta^{surf}}{\rho}, \text{ and} \\ \sigma_r &= -\frac{1}{3} \frac{1}{J^{SF}(\bar{\xi})} \frac{dJ^{SF}}{d\xi} \frac{E}{1-\nu} \frac{1}{r^2} \int_0^{\tilde{r}} \tilde{r} \Delta \xi d\tilde{r} - \frac{\sigma_\theta^{surf}}{\rho}, \end{aligned} \right\} \quad (7)$$

where  $\tilde{r} \equiv r/\rho$  is the dimensionless spatial coordinate;  $\rho = \rho(t) \approx [J^{SF}(\bar{\xi})]^{1/3} \rho_0$  can be approximated by the radius of the NW in the uniformly expanded configuration  $\mathbf{F}_0$ . The surface stress effect is included in Eq. (7).

The cylindrical symmetry of the NW dictates that  $\mathbf{j}^{Li} = j_r^{Li} \mathbf{e}_r$ . Equations (1), (3), (4), and (7) combine to give

$$\tilde{j}_r^{Li} = - \left( \frac{\Phi^{Li}(\bar{\xi})}{1+\bar{\xi}} + \xi \tilde{D}_{stress}^{Li} \right) \frac{\partial \xi}{\partial \tilde{r}} \approx - \left( \frac{\Phi^{Li}(\bar{\xi})}{1+\bar{\xi}} + \bar{\xi} \tilde{D}_{stress}^{Li} \right) \frac{\partial \xi}{\partial \tilde{r}}, \quad (8)$$

where  $\tilde{j}_r^{Li} \equiv \rho J^{SF}(\bar{\xi}) j_r^{Li} / D^{Li} C^{Si}$  is the dimensionless flux in the updated Lagrangian configuration,  $\tilde{D}_{stress}^{Li} \equiv (1/k_B \theta) \times (2E\eta^2/9(1-\nu))(1/J^{SF}(\bar{\xi}))(1/C^{Si})$  is the dimensionless effective diffusivity accounting for the contribution of stress to diffusion, and  $\Phi^{Li}(\bar{\xi}) \equiv 1 + \partial \ln \gamma^{Li} / \partial \ln x^{Li}$  is the stress-free thermodynamic factor.<sup>23</sup>  $\Phi^{Li}$  can be determined by the open-circuit potential (OCP)  $U^{OCP}$  of a stress-free Li/Si anode versus lithium metal through  $\Phi^{Li} = -(e/k_B \theta) \xi (1 + \xi) dU^{OCP} / d\xi$ , where  $e$  is the charge of a single electron. The approximation in Eq. (8) is due to the fact that  $\Delta \xi = \xi - \bar{\xi}$  is assumed to be small. The accuracy of this approximation is confirmed by separate numerical calculations.

Conservation of mass requires that  $\partial c^{Li} / \partial t = -(1/r) \partial (r j_r^{Li}) / \partial r$ . Therefore,

$$\frac{\partial \xi}{\partial t} = \frac{D_{eff}^{Li}}{\rho^2} \frac{1}{\tilde{r}} \frac{\partial}{\partial \tilde{r}} \left( \tilde{r} \frac{\partial \xi}{\partial \tilde{r}} \right) \text{ for } \tilde{r} \leq 1, \quad (9)$$

where  $D_{eff}^{Li} \equiv D^{Li} [\Phi^{Li}(\bar{\xi}) / (1+\bar{\xi}) + \bar{\xi} \tilde{D}_{stress}^{Li}]$  is the effective diffusivity. The boundary condition implied in (1) and (2) is

$$\tilde{j}_r^{Li} = -\frac{1}{2} \frac{\rho^2}{D^{Li}} \frac{\xi_{max}}{T_0} \text{ at } \tilde{r} = 1. \quad (10)$$

The transient solution to Eq. (9) under the condition of Eq. (10) is

$$\Delta \xi = \xi - \bar{\xi} = 2 \sum_{n=1}^{\infty} \left[ \frac{J_0(\lambda_n \tilde{r})}{J_0(\lambda_n)} \int_0^{\tilde{r}} e^{-\lambda_n^2 \tau} \tilde{j}_s(\tilde{r} - \tau) d\tau \right], \quad (11)$$

where  $\tilde{\tau} \equiv \tau / t_0 \equiv \int_0^t D_{eff}^{Li} / \rho^2 dt$  and  $\tilde{j}_s \equiv \rho^2 \xi_{max} / (2D_{eff}^{Li} T_0)$ .  $J_0(\tilde{r})$  is zeroth-order Bessel function of the first kind;  $\lambda_n$  is the  $n$ th root of the first-order Bessel function, i.e.,  $J_1(\lambda_n) = 0$ . Due to the exponential terms of  $\exp(-\lambda_n^2 \tau)$ , the transient solution would asymptotically approach its long-term behavior when  $t \gg t_0$ , where  $t_0 \equiv \rho_0^2 / \lambda_1^2 D^{Li}$  is the characteristic time for diffusion in the NW. To be specific, it is expected that  $\partial \xi / \partial t \approx \partial \bar{\xi} / \partial t = \xi_{max} / T_0$ , which leads to the long-term solution of

$$\xi = \xi_{max} \frac{t}{T_0} + \frac{1}{4} \frac{\rho^2}{D_{eff}^{Li}} \frac{\xi_{max}}{T_0} \left( \tilde{r}^2 - \frac{1}{2} \right). \quad (12)$$

### III. RESULTS AND DISCUSSIONS

Figure 2 shows the short-term concentration and stress

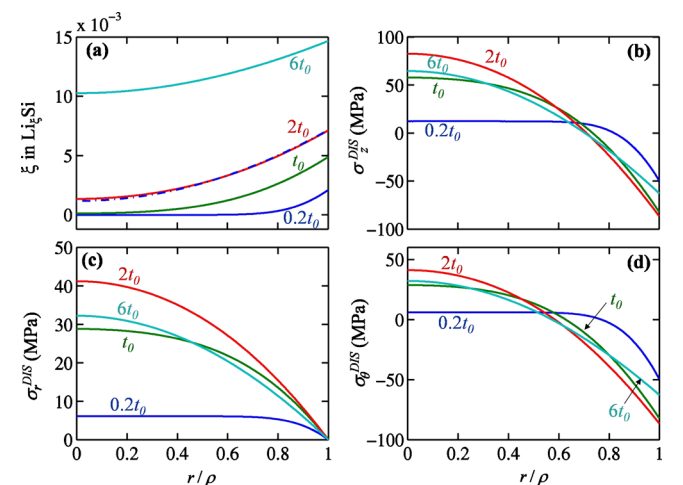


FIG. 2. (Color online) Short-term response of a Li<sub>5</sub>Si NW during the initial stages of a galvanostatic charge, (a) evolution of concentration distribution—the short-term solution (solid lines) quickly approaches the long-term solution (dotted line) by  $2t_0$ , (b)–(d)  $\sigma^{DIS} = \boldsymbol{\sigma} - \boldsymbol{\sigma}^0$  profiles. The NW diameter is 100 nm and the charging rate is 1 C.

profiles for a  $\text{Li}_\xi\text{Si}$  NW with an initial diameter of 100 nm at a charging rate of 1 C (full charge to  $\xi_{\max}$  in 1 h). Relevant material parameters are  $\xi_{\max}=4.4$ ,<sup>4</sup>  $C^{\text{Si}}=49.3$  atoms/nm<sup>3</sup> (pure amorphous Si with mass density  $\rho^{\text{Si}}=2.30$  g/cm<sup>3</sup>),<sup>24</sup>  $\eta=0.707$ , and  $D^{\text{Li}}=10^{-12}$  cm<sup>2</sup> s<sup>-1</sup>.<sup>25</sup> The concentration-dependent elastic properties are  $E=E(\bar{\xi})=(18.90\bar{\xi}+90.13)/(1+\bar{\xi})$  GPa and  $\nu=\nu(\bar{\xi})=(0.24\bar{\xi}+0.28)/(1+\bar{\xi})$ .<sup>26</sup>  $\Phi^{\text{Li}}=1$  for the dilute regime. To the best of the authors' knowledge, accurate surface stress data for  $\text{Li}_\xi\text{Si}$  is not currently available. An estimate through surface energy  $\gamma$  based on Kelly's approximation suggests that  $\sigma_\theta^{\text{surf}} \approx \sigma_z^{\text{surf}} \sim \gamma \sim Ea_0/10$ ,<sup>12,27</sup> with  $a_0$  being the equilibrium separation between two atomic planes. A typical value of  $\gamma$  is around 1 J/m<sup>2</sup>, which leads to  $\sigma_r^0 = \sigma_\theta^0 \sim -(\gamma/\rho_0) = -20$  MPa and  $\sigma_z^0 \sim -(2\gamma/\rho_0) = -40$  MPa for  $\rho_0=50$  nm. Since the stress contribution due to surfaces  $\sigma^0$  is compressive, the surface effect reduces tensile stresses during cycling. As pointed out by Cheng *et al.*,<sup>28</sup> this reduction in tensile stress may be partly responsible for the enhanced resistance to fracture and decrepitation of nanosized electrodes. To avoid the uncertainty associated with the value for  $\gamma$  and focus on the SED mechanism, only DIS due to concentration inhomogeneity  $\sigma^{\text{DIS}} \equiv \sigma - \sigma^0$  instead of the total stress  $\sigma$  is plotted here. Since  $\sigma^0$  is homogeneous throughout the wire [cf. Eq. (5)], the total stress  $\sigma$  can be readily obtained by shifting the  $\sigma^{\text{DIS}}$  curves. What is important here is to realize that  $\sigma^0$  has no bearing on diffusion.

The first observation from Fig. 2(a) is that the variation in  $\Delta\xi$  across the NW cross section is indeed small ( $|\Delta\xi| \sim 3 \times 10^{-3}$ ), validating the assumption made at the beginning. The smallness of  $|\Delta\xi|$  is also confirmed by a large-deformation full-coupling finite element simulation which will be reported in a separate publication. The short-term profiles for  $\xi$  approach quickly the long-term profile [Eq. (12)] after  $2t_0$ , where  $t_0 = \rho_0^2 / \lambda_1^2 D^{\text{Li}} = 1.7$  s is the characteris-

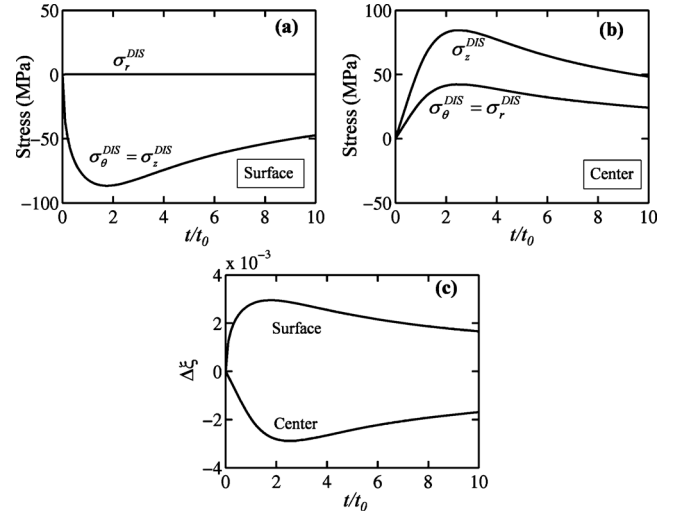


FIG. 3. [(a) and (b)] Stress evolution at the NW surface and center. (c)  $\Delta\xi = \xi - \bar{\xi}$  at the NW surface and center.  $t_0$  is the characteristic time for diffusion in the NW. The NW diameter is 100 nm and the charging rate is 1C.

tic time for diffusion for the wire at hand. Initially,  $\Delta\xi = \xi - \bar{\xi}$  increases with time but starts to decrease as the stress effect kicks in via  $\bar{\xi} \tilde{D}_{stress}^{\text{Li}}$  in  $D_{eff}^{\text{Li}}$ . Since  $\tilde{D}_{stress}^{\text{Li}}$  is always positive, the stress effect always increases the effective diffusivity  $D_{eff}^{\text{Li}}$  and thus enhances diffusion. The enhancement becomes more significant as  $\bar{\xi}$  increases. The result is that the stresses first increase and then decrease as  $\Delta\xi$  builds up and then decreases. As illustrated in Figs. 2(b)–2(d), the stresses are lower at  $6t_0$  than at  $2t_0$ .

Figure 3 shows the evolution of stresses at the NW surface and center, where the stress levels of  $\sigma^{\text{DIS}}$  are at their corresponding extreme values. Since  $(1/\bar{r}^2) \int_0^{\bar{r}} \Delta\xi d\bar{r} = 0$  at  $\bar{r} = 1$  (surface) and  $\lim_{\bar{r} \rightarrow 0} (1/\bar{r}^2) \int_0^{\bar{r}} \bar{r} \Delta\xi d\bar{r} = \Delta\xi/2$  (center), Eq. (7) simplifies into

$$\left. \begin{aligned} \sigma_\theta^{\text{DIS}} = \sigma_z^{\text{DIS}} = -\frac{1}{3} \frac{1}{J^{SF}(\bar{\xi})} \frac{dJ^{SF}}{d\xi} \frac{E}{1-\nu} \Delta\xi \text{ and } \sigma_r^{\text{DIS}} = 0 \text{ at } r \rightarrow \rho, \text{ and} \\ \sigma_z^{\text{DIS}} = -\frac{1}{3} \frac{1}{J^{SF}(\bar{\xi})} \frac{dJ^{SF}}{d\xi} \frac{E}{1-\nu} \Delta\xi \text{ and } \sigma_\theta^{\text{DIS}} = \sigma_r^{\text{DIS}} = \frac{\sigma_z^{\text{DIS}}}{2} \text{ at } r = 0. \end{aligned} \right\} \quad (13)$$

After a quick initial increase,  $\sigma^{\text{DIS}}$  at the surface levels off and reaches a maximum at  $t \approx 2t_0$  as illustrated in Fig. 3(a). The evolution of  $\sigma^{\text{DIS}}$  at the NW center lags due to the time needed for concentration to propagate from surface to center. The subsequent decrease in the stresses at both the surface and center (and throughout the NW) after the full development of  $\Delta\xi$  is due to the effect of SED through the term  $\bar{\xi} \tilde{D}_{stress}^{\text{Li}}$  in  $D_{eff}^{\text{Li}}$ . A close look at Eqs. (7), (11), and (13) also reveals that the maximum DIS at the center and surface approximately scale with  $\rho_0^2 / D^{\text{Li}} T_0$ .

Figure 4 shows the long-term concentration and stress profiles for the same  $\text{Li}_\xi\text{Si}$  NW under the same charging rate as in Fig. 3 at a state of charge (SOC) of  $\xi/\xi_{\max}=0.5$ . Ding's experiments<sup>25</sup> suggest that  $dU^{\text{OCP}}/d\xi \approx -0.1$  eV at  $\xi = 0.5\xi_{\max} = 2.2$ , leading to  $\Phi^{\text{Li}}(\bar{\xi}) = 27.2$ . Again, the variation in  $\Delta\xi$  across the NW cross section is small, validating the assumption made at the beginning. To reveal the significance of SED at this intermediate SOC, both solutions with and without  $\tilde{D}_{stress}^{\text{Li}}$  in  $D_{eff}^{\text{Li}} \equiv D^{\text{Li}} [\Phi^{\text{Li}}(\bar{\xi}) / (1 + \bar{\xi}) + \bar{\xi} \tilde{D}_{stress}^{\text{Li}}]$  are shown. Obviously, the SED effect significantly enhances the

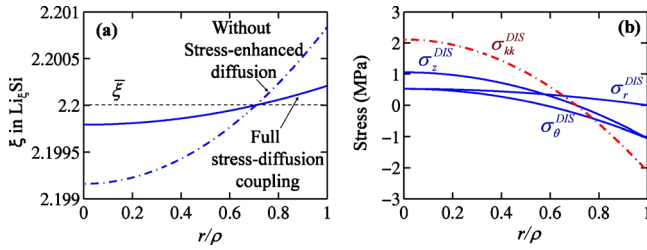


FIG. 4. (Color online) Long-term solution for a  $\text{Li}_x\text{Si}$  NW when charged to a SOC of  $\bar{\xi}=0.5\xi_{\text{max}}=2.2$ . (a) concentration and (b) stress. The NW diameter is 100 nm and the charging rate is 1C.

diffusion process, making  $\xi$  much more uniform. This effect amounts to an increase in  $\bar{\xi}\bar{D}_{\text{stress}}^{\text{Li}}/[\Phi^{\text{Li}}/(1+\bar{\xi})]=303\%$  in the effective diffusivity of lithium. The long-term DIS profiles in Fig. 4(b) offer insight as well. The radial stress  $\sigma_r^{\text{DIS}}$  is tensile throughout the wire. On the other hand, the axial stress  $\sigma_z^{\text{DIS}}$  and the hoop stress  $\sigma_\theta^{\text{DIS}}$  are tensile in the core and compressive near the surface. The hydrostatic part of  $\sigma^{\text{DIS}}$  is only  $\sim 2$  MPa in a thin wire with  $d=100$  nm under a moderate charging rate of 1 C. Nevertheless, such a low DIS level contributes significantly to the overall driving force for diffusion as seen in Fig. 4(a).

Equations (7) and (12) show that the long-term DIS  $\sigma^{\text{DIS}} \propto \Delta\xi \propto \rho^2/D_{\text{eff}}^{\text{Li}}T_0$ . Thus, the long-term stresses also increase quadratically with the wire radius and are inversely related to the charging rate and the diffusivity. These scaling relations are consistent with previous findings of Christensen *et al.*<sup>8</sup> for  $\text{LiC}_6$  and Zhang *et al.*<sup>13</sup> for  $\text{LiMn}_2\text{O}_4$ . What is different here is the strong modulation of the effective diffusivity by  $\bar{\xi}\bar{D}_{\text{stress}}^{\text{Li}}$  in the case of  $\text{Li}_x\text{Si}$ . Zhang *et al.*<sup>13</sup> discussed the effect of SED of Li in  $\text{Mn}_2\text{O}_4$  crystalline cathodes and showed that the difference in concentration inhomogeneity  $\max(\Delta\xi)=\xi(\rho)-\bar{\xi}$  with and without the SED effect is  $\sim 13\%$ ; for  $\text{LiC}_6$  the difference is  $\sim 20\%$ .<sup>8</sup> Here, however, the difference is 303%. The enhancement due to stress in  $\text{Li}_x\text{Si}$  is much more pronounced for two reasons. First, the partial atomic volume  $\Omega=\eta/C^{\text{Si}}$  of lithium in  $\text{Li}_x\text{Si}$  is  $14.3 \text{ \AA}^3$ , much larger than the partial atomic volume of Li in  $\text{Mn}_2\text{O}_4$  [ $\Omega=5.8 \text{ \AA}^3$  per Li (Ref. 13)]. The lower amount of open space in the alloy electrodes compared with that in intercalation lattices gives rise to the stronger SED effect seen in Fig. 3. Second,  $\text{Li}_x\text{Si}$  can be charged to a much higher Li concentration limit than cathode lattices and the contribution of stress to effective diffusivity ( $\bar{\xi}\bar{D}_{\text{stress}}^{\text{Li}}$ ) is proportional to the average concentration  $\bar{\xi}$ . It should be noted that the change of  $D^{\text{Li}}$  with stress is not considered in this paper. Haftbaradaran *et al.*<sup>15</sup> considered the activation barrier shift  $\Delta E_b$  for diffusion due to DIS and showed that the stress effect could slow down diffusion through  $D^{\text{Li}}=D_0^{\text{Li}}\exp(-\Delta E_b/k_B\theta)$ . While stress-induced activation barrier change  $\Delta E_b$  is more important under very high stresses, stress development and diffusion mainly couple through the chemical potential for moderate stresses<sup>29</sup> which is the regime we consider in this paper. There might be a transition threshold below which stress enhances diffusion and above which stress hinders diffusion. Following Haftbaradaran *et al.*,<sup>15</sup> we take  $\alpha=0.3$  for  $\Delta E_b=-\alpha\Omega\sigma_b$  where  $\sigma_b$  is the bi-axial surface

stress. This leads to  $|\Delta E_b/k_B\theta| \approx 1$  only when  $|\sigma_b|$  reaches as high as 1 GPa, otherwise, the factor  $\exp(-\Delta E_b/k_B\theta)$  is negligible. Therefore, if a transition threshold exists, it must be very high, even comparable to the yield stress for onset of plasticity.<sup>30</sup>

The levels of  $\sigma^{\text{DIS}}$  at the lower concentrations in Fig. 2 and 3 are as much as  $\sim 100$  times those at the higher concentrations in Fig. 4. To understand this significant change in stress levels, note that  $\Phi^{\text{Li}}(\bar{\xi})/(1+\bar{\xi})=8.5$  and  $\bar{\xi}\bar{D}_{\text{stress}}^{\text{Li}}=25.8$  at  $t=T_0/2$  ( $\bar{\xi}=2.2$ ) and  $\Phi^{\text{Li}}(\bar{\xi})/(1+\bar{\xi}) \approx 1$  and  $\bar{\xi}\bar{D}_{\text{stress}}^{\text{Li}}=0.14$  at  $t=2t_0$  ( $\bar{\xi}=2.1 \times 10^{-3}$ ) for  $\text{Li}_x\text{Si}$ . Also contributing to this is the fact that the material is softer (as measured by the elastic modulus) at higher lithium concentrations.<sup>26</sup> The thermodynamic factor enhancement, SED and the softening of material lead to lower stress levels at higher Li concentrations. In this process, the SED effect is the dominant factor and the most important. It should be noted that experimentally measured  $U^{\text{OCP}}(\xi)$  curves for  $\text{Li}_x\text{Si}$  are associated with significant hysteresis<sup>31</sup> which makes accurate estimates of the quasi-equilibrium value of  $dU^{\text{OCP}}/d\xi$  difficult. This lack of accuracy in determining the value of  $dU^{\text{OCP}}/d\xi$  should not be construed as to obscure the importance of SED in the intermediate composition range. For example, even if  $|dU^{\text{OCP}}/d\xi|=0.15$  eV,  $\Phi^{\text{Li}}(\bar{\xi})/(1+\bar{\xi})=12.8$  and  $\bar{\xi}\bar{D}_{\text{stress}}^{\text{Li}}/[\Phi^{\text{Li}}/(1+\bar{\xi})]=202\%$ , a scenario in which SED still dominates.

If the NW radius is large or charging rate is high, the total stress  $\sigma=\sigma^{\text{DIS}}+\sigma^0$  could be high enough to cause material failure. The fact that the peak DIS levels scale with  $\rho_0^2/D^{\text{Li}}T_0$  and the initial DIS levels are much higher than the long-term values suggests that lower charging rates should be used to prime a new Si anode or a Si anode after deep discharge in order to avoid mechanical failure during initial charging. The results obtained here also indicate that deep discharging would reduce the cyclability of  $\text{Li}_x\text{Si}$  anodes because of the higher DIS at low concentrations. The adverse effect is more pronounced if fast recharge is carried out subsequently.

## IV. CONCLUSIONS

The development of DIS in amorphous  $\text{Li}_x\text{Si}$  alloy NW-based electrodes is analyzed using a finite deformation framework, accounting for full two-way diffusion-stress development coupling. Analytical solutions for concentration and stresses are obtained via linearization through a perturbation method. Significant contribution to diffusion by stress at high Li concentrations is shown for  $\text{Li}_x\text{Si}$  electrodes. The contribution of stress to diffusion is small when Li concentration is low in early stages of a charging process, leading to high DIS levels. A rational charging regimen for Li ion batteries with new amorphous Si anodes should include priming with a charging rate significantly lower than the regular operational charging rate. The analysis also suggests that deep discharging should be avoided, especially when fast recharges are needed subsequently. The long-term DIS levels scale with NW radius, charging rate, and stress-modulated Li mobility in Si, reflecting the strong two-way coupling be-

tween diffusion and stress development, in contrast to what is the case for most intercalation electrodes. The scaling law suggests that designs that take advantage of the size effect, controlling of charging rate and enhancement of diffusion through alloying are all effective means for enhancing the reliability of  $\text{Li}_6\text{Si}$  anodes.

## ACKNOWLEDGMENTS

Support from the National Research Foundation (NRF) of Korea through World Class University (WCU) program Grant No. R31-2008-000-10083-0 is gratefully acknowledged.

<sup>1</sup>D. Larcher, S. Beattie, M. Morcrette, K. Edstroem, J. C. Jumas, and J. M. Tarascon, *J. Mater. Chem.* **17**, 3759 (2007).

<sup>2</sup>V. L. Chevrier and J. R. Dahn, *J. Electrochem. Soc.* **156**, A454 (2009).

<sup>3</sup>L. Y. Beaulieu, K. W. Eberman, R. L. Turner, L. J. Krause, and J. R. Dahn, *Electrochem. Solid-State Lett.* **4**, A137 (2001).

<sup>4</sup>C. K. Chan, H. L. Peng, G. Liu, K. McIlwrath, X. F. Zhang, R. A. Huggins, and Y. Cui, *Nat. Nanotechnol.* **3**, 31 (2008).

<sup>5</sup>L. F. Cui, R. Ruffo, C. K. Chan, H. L. Peng, and Y. Cui, *Nano Lett.* **9**, 491 (2009).

<sup>6</sup>T. Song, J. L. Xia, J. H. Lee, D. H. Lee, M. S. Kwon, J. M. Choi, J. Wu, S. K. Doo, H. Chang, W. Il Park, D. S. Zang, H. Kim, Y. G. Huang, K. C. Hwang, J. A. Rogers, and U. Paik, *Nano Lett.* **10**, 1710 (2010).

<sup>7</sup>A. Magasinski, P. Dixon, B. Hertzberg, A. Kvit, J. Ayala, and G. Yushin, *Nature Mater.* **9**, 353 (2010).

<sup>8</sup>J. Christensen and J. Newman, *J. Solid State Electrochem.* **10**, 293 (2006).

<sup>9</sup>J. Christensen, *J. Electrochem. Soc.* **157**, A366 (2010).

<sup>10</sup>Y. T. Cheng and M. W. Verbrugge, *J. Appl. Phys.* **104**, 083521 (2008).

<sup>11</sup>Y. T. Cheng and M. W. Verbrugge, *J. Power Sources* **190**, 453 (2009).

<sup>12</sup>R. Deshpande, Y. T. Cheng, and M. W. Verbrugge, *J. Power Sources* **195**, 5081 (2010).

<sup>13</sup>X. C. Zhang, W. Shyy, and A. M. Sastry, *J. Electrochem. Soc.* **154**, A910 (2007).

<sup>14</sup>T. K. Bhandakkar and H. J. Gao, *Int. J. Solids Struct.* **47**, 1424 (2010).

<sup>15</sup>H. Hafitbaradaran, H. J. Gao, and W. A. Curtin, *Appl. Phys. Lett.* **96**, 091909 (2010).

<sup>16</sup>C. H. Wu, *J. Mech. Phys. Solids* **49**, 1771 (2001).

<sup>17</sup>H. El Kadiri, M. F. Horstemeyer, and D. J. Bammann, *J. Mech. Phys. Solids* **56**, 3392 (2008).

<sup>18</sup>H. G. Zhou, J. M. Qu, and M. Cherkaoui, *Mech. Mater.* **42**, 63 (2010).

<sup>19</sup>N. Swaminathan, J. Qu, and Y. Sun, *Philos. Mag.* **87**, 1705 (2007).

<sup>20</sup>N. Swaminathan and J. Qu, *Fuel Cells* **7**, 453 (2007).

<sup>21</sup>L. Y. Beaulieu, T. D. Hatchard, A. Bonakdarpour, M. D. Fleischauer, and J. R. Dahn, *J. Electrochem. Soc.* **150**, A1457 (2003).

<sup>22</sup>S. Timoshenko, *Theory of Elasticity*, 2nd ed. (McGraw-Hill, New York, 1951).

<sup>23</sup>J. S. Newman and K. E. Thomas-Alyea, *Electrochemical Systems*, 3rd ed. (Wiley, New York, 2004).

<sup>24</sup>M. Szabadi, P. Hess, A. J. Kellock, H. Coufal, and J. E. E. Baglin, *Phys. Rev. B* **58**, 8941 (1998).

<sup>25</sup>N. Ding, J. Xu, Y. X. Yao, G. Wegner, X. Fang, C. H. Chen, and I. Lieberwirth, *Solid State Ionics* **180**, 222 (2009).

<sup>26</sup>V. B. Shenoy, P. Johari, and Y. Qi, *J. Power Sources* **195**, 6825 (2010).

<sup>27</sup>A. Kelly, *Strong Solids*, 2nd ed. (Clarendon, Oxford, 1973).

<sup>28</sup>Y. T. Cheng and M. W. Verbrugge, *J. Electrochem. Soc.* **157**, A508 (2010).

<sup>29</sup>H. H. Yu and Z. Suo, *J. Appl. Phys.* **87**, 1211 (2000).

<sup>30</sup>V. A. Sethuraman, M. J. Chon, M. Shimshak, V. Srinivasan, and P. R. Guduru, *J. Power Sources* **195**, 5062 (2010).

<sup>31</sup>V. L. Chevrier and J. R. Dahn, *J. Electrochem. Soc.* **157**, A392 (2010).